Early Evolution of the Stratospheric Aerosol Plume Following the 2022 Hunga Tonga-Hunga Ha'apai Eruption: Lidar Observations From Reunion (21°S, 55°E)

A. Baron, P. Chazette, Sergey Khaykin, G. Payen, N. Marquestaut, N. Bègue, V. Duflot

Geophysical Research Letters

RESEARCH LETTER
10.1029/2022GL101751

Key Points:

- Record-breaking altitude of a volcanic plume observed by a ground-based lidar
- Unprecedented aerosol optical depth and extinction values observed in the stratosphere
- Evidence of aerosol layers with higher extinction efficiency at 532 nm than at 355 nm

Supporting Information:

Supporting Information may be found in the online version of this article.

Correspondence to:

A. Baron,
alexandre.baron@noaa.gov

Citation:

Baron, A., Chazette, P., Khaykin, S., Payen, G., Marquestaut, N., Bègue, N., & Duflot, V. (2023). Early evolution of the stratospheric aerosol plume following the 2022 Hunga Tonga-Hunga Ha'apai eruption: Lidar observations from Reunion (21°S, 55°E). *Geophysical Research Letters*, *50*, e2022GL101751. https://doi.org/10.1029/2022GL101751

Received 17 OCT 2022
Accepted 15 APR 2023

Author Contributions:

Conceptualization: A. Baron, P. Chazette, S. Khaykin, V. Duflot
Data curation: A. Baron
Formal analysis: A. Baron
Funding acquisition: V. Duflot
Investigation: A. Baron
Methodology: A. Baron, P. Chazette
Project Administration: V. Duflot
Resources: A. Baron, G. Payen, N. Marquestaut
Software: A. Baron, G. Payen
Supervision: A. Baron, P. Chazette, S. Khaykin, V. Duflot
Validation: A. Baron, P. Chazette, N. Bègue, V. Duflot
Visualization: A. Baron

Early Evolution of the Stratospheric Aerosol Plume Following the 2022 Hunga Tonga-Hunga Ha'apai Eruption: Lidar Observations From Reunion (21°S, 55°E)

A. Baron[1,2,3], P. Chazette[4], S. Khaykin[5], G. Payen[6], N. Marquestaut[6], N. Bègue[1], and V. Duflot[1]

[1]Laboratoire de l'Atmosphère et des Cyclones (LACy), UMR 8105 CNRS, Université de la Réunion, Météo-France, Saint-Denis de La Réunion, France, [2]Now at Cooperative Institute for Research in Environmental Sciences, CU Boulder, Boulder, CO, USA, [3]Now at NOAA Chemical Sciences Laboratory, Boulder, CO, USA, [4]Laboratoire des Sciences du Climat et de l'Environnement, LSCE-IPSL, UMR 8212, Université Paris-Saclay, CEA, CNRS, UVSQ, Gif-sur-Yvette, France, [5]Laboratoire Atmosphère Milieux Observations Spatiales, LATMOS-IPSL, UMR 8190, Sorbonne Université, UVSQ, CNRS, Paris, France, [6]Observatoire des Sciences de l'Univers de La Réunion (OSU-Réunion), UAR 3365, Université de la Réunion, CNRS, Météo-France, Saint-Denis de La Réunion, France

Abstract The exceptionally violent eruption of the Hunga Tonga-Hunga Ha'apai volcano (HTHH) of 15 January 2022, in the South Pacific, was associated with a powerful blast that injected gases, steam and aerosol to unprecedentedly high altitudes. This article details unique observations of the young volcanic plume from ground-based lidars at Reunion (21°S, 55°E). Two lidars, operating at wavelengths of 355 and 532 nm, recorded the plume overhead from 19 January until 28 January providing the vertical structure and the optical properties of the plume. A series of thick stratospheric plumes between 36 and 18 km altitude have been characterized along time, with aerosol optical depth as high as 0.84 at 532 nm and negative Angström exponents for the main layers down to -0.8 ± 0.8. The diversity of plumes properties is explained by the injection heights of the volcanic material as well as stratospheric dynamics and chemistry.

Plain Language Summary In January 2022, the Hunga Tonga-Hunga Ha'apai (HTHH) underwater volcano exploded in the southern Pacific (20.5°S, 175.4°W). Eruption metrics of this outbreak is to be compared to historic climate impacting volcanic events of the past century (e.g., Mount Pinatubo). Based on laser remote-sensing observations of the HTHH plume, its early structural and optical properties were assessed during its passage over Reunion (21°S, 55°E). Our results show record-breaking optical characteristics for such high altitudes, deep in the stratosphere between 18 and 36 km. In particular, peak values of aerosol optical thickness which represents the opacity of the atmosphere, were never recorded as high. Moreover, although this property is expected to decrease with increasing wavelength of the light spectrum, the thickest aerosol layers we recorded show a different optical behavior. They are opaquer in the visible spectrum around 532 nm than in the UV at 355 nm. This is likely to be link to the specific size distribution of these volcanic particles, driven by an unusual stratospheric chemistry resulting from the presence of large amount of water vapor. These findings are original and essential observations to question our understanding of such atmospheric processes and to help improve global climate models.

1. Introduction

Knowledge about climate response to large injections of aerosols in the stratosphere comes from observations and modeling of (a) historic volcanic eruptions (e.g., Robock, 2015) that occurred periodically (Delmas et al., 1992; Tejedor et al., 2021) and (b) extreme wildfires generating pyroconvection processes able to inject carbon-rich aerosols into the lower stratosphere (Khaykin et al., 2020; Yu et al., 2019). Only three major eruptions have occurred in the 20th century: Mount Agung, El Chichon and Mount Pinatubo. All three were characterized by a Volcanic Explosivity Index (VEI) ≥5 and followed by a significant and durable decrease of the tropospheric and surface temperatures (Angell, 1993; Robock & Mao, 1995). The most recent was the eruption of Mount Pinatubo in 1991, abundantly documented through observational and modeling studies (Boville et al., 1991; DeFoor et al., 1992; Gobbi et al., 1992; Graft et al., 1993; McCormick et al., 1995; Minnis et al., 1993). However, it is still difficult to model quantitatively the amount of volcanic material injected to match observations (Dhomse et al., 2020; Guo et al., 2004; McCormick & Veiga, 1992).

Writing – original draft: A. Baron
Writing – review & editing: A. Baron, P. Chazette, S. Khaykin, G. Payen, N. Marquestaut, N. Bègue, V. Duflot

To improve the accuracy of climate models, observations should provide reliable altitude of plumes which is critical for aerosol residence time and atmospheric stability (Krishnamohan et al., 2019), as well as reliable optical properties, crucial for direct radiative effects. These observations can be jointly provided by satellite and ground-based stations measurements used in complementarity.

The aftermath of the eruption of the HTHH volcano is under extensive scrutiny since it occurred in the South Pacific (20.5°S, 175.4°W), on 15 January 2022. Its shallow underwater caldera has contributed to an extremely powerful blast triggering a phreatoplinian eruption (Yuen et al., 2022). The blast, estimated to range between 100 and 200 MT of TNT equivalent (Vergoz et al., 2022) generated a pressure wave recorded all around the globe (Amores et al., 2022; Podglajen et al., 2022) and a worldwide Tsunami (Carvajal et al., 2022). On the atmospheric side, the disturbance generated by the expulsion of water, ash and gas went as high as piercing the stratopause (Carr et al., 2022; Proud et al., 2022). While its VEI of almost 6 and the stratospheric perturbation induced certainly place this event in the same league as the very large eruptions recorded in the 20th century (Khaykin et al., 2022; Poli & Shapiro, 2022), the climatic impact of this event is somewhat unforeseen. As expected knowing the literature on volcanic impact on climate, the aerosol-only radiative impact is a surface cooling effect (Zhu et al., 2022). Yet, Sellitto et al. (2022) assessed that this well know umbrella effect is counterbalanced by the water-vapor warming effect within the atmosphere. This volcanic event is then a surprising outlier, warming the climate in a landscape of cooling major volcanic eruptions.

Following the westward zonal wind flow in the stratosphere, the volcanic material injected above the tropopause rapidly headed toward the Indian Ocean, stably centered around the 20°S latitude belt. Directly in the path of the plume, 12,800 km away from the Tonga archipelago, the French overseas territory of Reunion (21°S, 55°E) stands in the southwest of the Indian Ocean as its highest peak. This island hosts the Atmospheric Physics Observatory of Reunion (OPAR) from where we sampled the early evolution of the aerosol plume just 4 days after the eruption, while it was still weakly dispersed according to satellite observations (Legras et al., 2022). Such early observations have not been possible for past remarkable geophysical events of the 20th century: for HTHH, this data set will help to understand the key processes occurring in the fresh plume.

Two lidars have been operated for stratospheric aerosol measurements every night during the first overpass of the plume: from its arrival on 19 January, until 28 January. This sampling allows to assess both the vertical structures and the optical properties of the plume as it progresses zonally. Such data made it possible to constrain Mie modeling to draw some conclusions on the evolution of the particle size during the volcanic plume passage.

In the following, the technical aspects inherent to lidar systems and inversion protocol are shortly presented in Section 2. We then discuss the plume vertical structure in Section 3. The evolution of the plume optical properties are then examined in Section 4, before the discussion concluding this paper.

2. Instruments and Methods

2.1. OPAR Lidars

Within OPAR, the Maïdo Observatory (Baray et al., 2013) is a facility located on the Maïdo mount (2,160 m above the mean sea level—AMSL, lee side on the tropical island). Aerosol observations are performed routinely at Maïdo Observatory since 2013 thanks to two lidar systems: the LiO_3T and the Li1200. The Li1200 is dedicated to the measurement of water vapor in the troposphere and of aerosol in the troposphere and stratosphere (Dionisi et al., 2015; Vérèmes et al., 2019). It is based on two 30 Hz pulsed Nd:YAG lasers emitting at 355 nm with an energy per pulse equivalent to 800 mJ after beams-recombination. The reception system is composed of a 1,200 mm parabolic mirror (7.2 m effective focal length) and Licel electronics, which allow to record profiles every 1 min, with a vertical resolution downgraded to 15 m. The LiO_3T is dedicated to the measurement of ozone in the troposphere, and of aerosol in the troposphere and stratosphere (Duflot et al., 2017). The aerosol channel of the LiO_3T is based on a 30 Hz Nd:YAG laser emitting 532 nm pulses of 250 mJ, and a reception system composed of a 500 mm parabolic mirror (1.5 m focal length) and an optical fiber (1 mm diameter). The profiles are recorded every 2 min with a vertical resolution of 7.5 m.

For both lidar systems, the profiles are averaged over 5 min and 50 m before the retrieval of aerosol optical properties. Note that stratospheric measurements being above the overlap factors of both systems, they are not impacted.

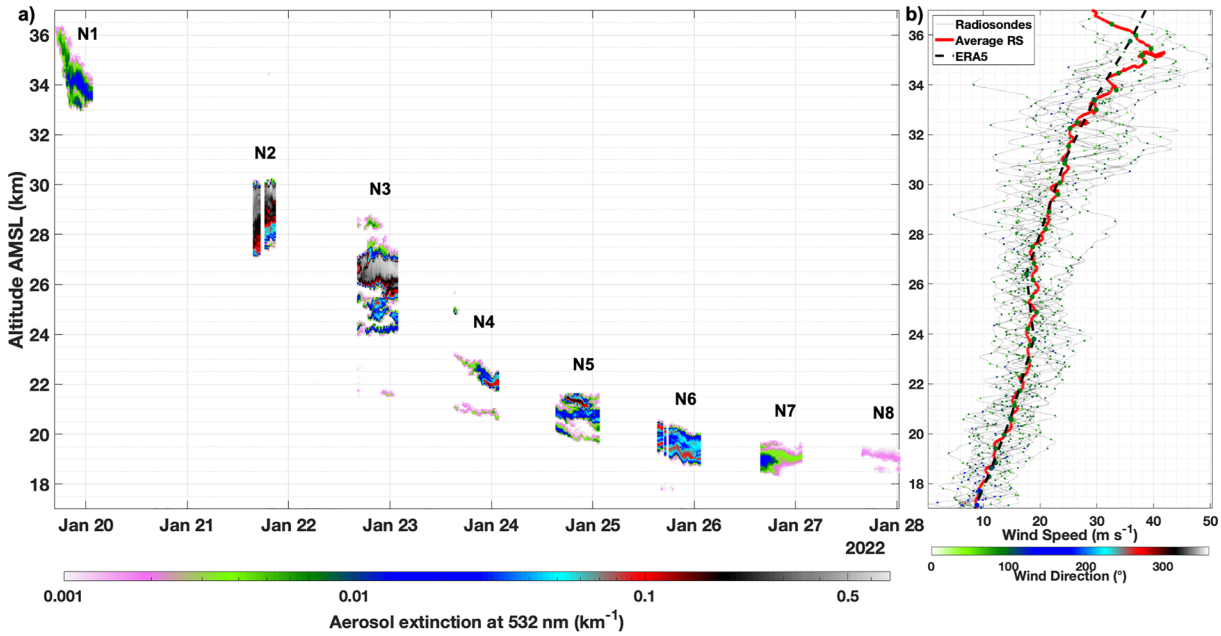

Figure 1. The time-altitude curtain of aerosol extinction coefficient at 532 nm is plotted (a) from 19 to 28 January. The layers are named from N1 to N8, corresponding to every night of observation showing a significant aerosol burden. Concomitant wind profiles are shown (b) from radiosondes (as pale gray lines, whilst a thick red line shows their average), and the output of ERA5 is superimposed (dashed black line). The color in (b) informs on the direction of the wind.

2.2. Retrieval of Optical Properties

In the stratosphere, the ratio of the total volume backscatter and the volume molecular backscatter coefficients is often used. Named scattering ratio (SR), a value of 1 corresponds to the molecular background and greater than 1 to an aerosol perturbation. Also, aerosol layers transported in the stratosphere are often sandwiched between aerosol-free air parcels, whose optical behavior follows the Rayleigh scattering framework. Using the transmittance method described in the literature (Chazette et al., 1995; Platt, 1973), it is then straightforward to compute the AOD of a stratospheric layer. The derived AOD is thereupon used as an input for an iterative Klett inversion method (Klett, 1985) to retrieve simultaneously the vertical profile of aerosol extinction coefficient (AEC) and the lidar ratio (LR). LR is namely the ratio of the aerosol extinction to backscatter coefficients, often ranging from 5 sr to slightly over 100 sr. It is often used to classify aerosol types (Chazette et al., 2016; Mallet et al., 2022; Müller et al., 2007) as it provides indications such as the size (lower LR being link to coarser particle size) and the absorption properties (the higher LR the more absorbent) of aerosols.

The available literature documenting lidar-derived properties above Reunion is scarce. Duflot et al. (2011) presented tropospheric LR values at 355 nm in the south-western Indian Ocean for marine aerosols (26 ± 6 sr) and a biomass burning plume (48 ± 12 sr). The present study shows for the first time LR and Angström exponent (AE) values retrieved by lidar over Reunion during a volcanic eruption event.

3. Structures of the Stratospheric Aerosol Plumes

Figure 1 shows the AEC of the different aerosol layers which overflew Reunion during the second half of January 2022 (Figure 1a). Each layer is named from N1 to N8.

Figure 1b shows the wind profile from local radiosondes and as reanalyzed by the European Center for Medium-Range Weather Forecast (ECMWF) through the ERA5 product at 0.25° resolution (Hersbach et al., 2020). We used an inverse-distance weighted average from the nine grid points surrounding Mount Maïdo to have collocated profiles, and proceeded to average these during the period of measurement.

The inverse comma shape noticeable on Figure 1a is typical of early observations of volcanic plumes transported over long distances (Chazette et al., 2012). Even if the HTHH eruption sequence presents several pulses (Podglajen et al., 2022), the event remains short (~20 hr). This shape results from a strong vertical gradient of

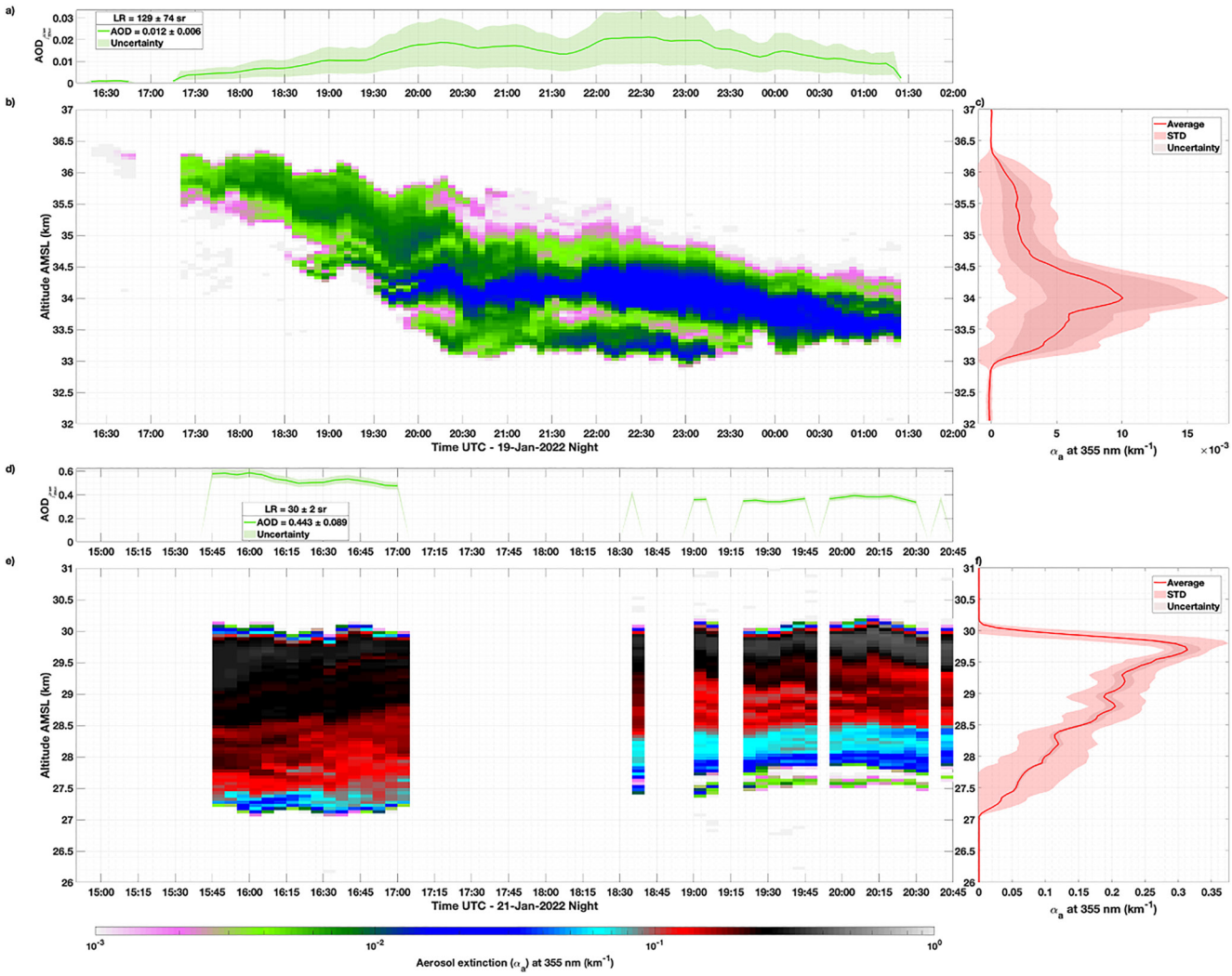

Figure 2. Lidar observations at 355 nm during 19 January (a–c) and 21 January (d–f). For both nights, the aerosol optical depth time series is displayed (a–d). The aerosol extinction coefficient (α_a) time-altitude curtain is plotted with a logscale colorbar (b–e) and the corresponding averaged profile is represented in red (c–f). The missing parts are screened cloudy profiles.

zonal wind bending the eruptive column through its transport in the stratosphere. Indeed, routine radiosondes in Reunion (Figure 1b) show a mainly zonal wind direction in the stratosphere with peak wind speed of 15 m s^{-1} around 18–20 km, a value which triples to 40–45 m s^{-1} at the altitude of the highest observed layer (35 km).

This high wind velocity in the mid-stratosphere (Legras et al., 2022) also explains the precocious arrival of the layer N1 sampled during the night of 19 to 20 January, between 33 and 36 km. It made the journey in 108 hr at an average cruising velocity of ∼33 m s^{-1}, a value which corresponds to Figure 1b, suggesting a stable flow along the way. These particles reached an impressive altitude which, to our knowledge, was never observed by ground-based instruments for a volcanic plume.

4. Temporal and Vertical Evolutions of the Aerosol Optical Properties

Although N1 is optically thin (max AEC ∼ 0.03 km^{-1} at 355 nm, see Figures 2a–2c) in contrast to the layers arriving afterward (especially N2 and N3, see Figures 2d–2f), it is still a significant aerosol load for the stratosphere, knowing that the AEC typical background is not exceeding 10^{-4} km^{-1} at these altitudes (Vernier et al., 2011).

Given its relatively low AEC, N1 was not easily observed from passive remote sensors onboard satellites. Nevertheless, it could be tracked by the Ozone Monitoring and Profiler Suite (Taha et al., 2022) on NASA's S-NPP

Table 1
Geometrical and Optical Characteristics of the Plume

Layers (January night)	Altitude range (peak) (km)	λ (nm)	AOD (max)	AEC peak (max) (km^{-1})	SR peak (max)	Lidar ratio (sr)	Angström exponent
N1 (19)	33–36 (34.1)	355	0.01 ± 0.01 (0.03)	0.01 ± 0.01 (0.03)	2.2 ± 1.0 (3.9)	129 ± 74	–
		532	–	–	5.8 ± 3.6 (12)	–	
N2 (21)	27–30 (29.7)	355	0.44 ± 0.10 (0.59)	0.31 ± 0.03 (0.41)	80 ± 9.0 (107)	30 ± 2	−0.8 ± 0.8
		532	0.60 ± 0.15 (0.84)	0.45 ± 0.05 (0.66)	272 ± 33 (404)	69 ± 11	
N3 (22)	24–28 (26.8)	355	0.31 ± 0.09 (0.43)	0.30 ± 0.09 (0.41)	45 ± 13 (61)	33 ± 6	−0.7 ± 0.9
		532	0.41 ± 0.10 (0.55)	0.43 ± 0.14 (0.63)	150 ± 50 (218)	75 ± 7	
N4 (23)	21–23 (22.1)	355	0.01 ± 0.01 (0.04)	0.03 ± 0.04 (0.12)	3.0 ± 3.1 (10)	29 ± 5	0.0 ± 3.5
		532	0.01 ± 0.01 (0.04)	0.03 ± 0.04 (0.13)	6.7 ± 9.0 (29)	57 ± 15	
N5 (24)	20–22 (21.3)	355	0.03 ± 0.02 (0.05)	0.06 ± 0.06 (0.18)	4.2 ± 3.7 (11)	35 ± 7	0.0 ± 1.8
		532	0.03 ± 0.01 (0.05)	0.06 ± 0.07 (0.19)	10 ± 11 (34)	63 ± 11	
N6 (25)	19–21 (19.3)	355	0.08 ± 0.01 (0.10)	0.09 ± 0.03 (0.16)	3.6 ± 0.8 (6.4)	46 ± 10	1.2 ± 0.6
		532	0.05 ± 0.01 (0.06)	0.06 ± 0.02 (0.11)	7.4 ± 1.8 (16)	65 ± 9	
N7 (26)	18–20 (19.1)	355	0.01 ± 0.01 (0.03)	0.02 ± 0.02 (0.06)	1.6 ± 0.5 (2.6)	44 ± 8	–
		532	–	–	2.7 ± 1.3 (5.3)	–	
N8 (27)	18–20 (19.1)	355	–	–	1.5 ± 0.1 (1.6)	–	–
		532	–	–	2.2 ± 0.1 (2.4)	–	

Note. AOD stands for Aerosol Optical Depth, AEC for Aerosol Extinction Coefficient and SR for Scattering Ratio. The values given are night averaged with associated standard deviations. The maximum is also added in parentheses as well as the altitude where the peak can be found. Note that for N1, N7, and N8 at 532 nm as well as for N8 at 355 nm, only attenuated SR are provided for insufficient signal reasons.

satellite. The spaceborne lidar CALIOP onboard CALIPSO (Winker et al., 2003) also observed this tenuous layer between 35 and 40 km during its orbit between Australia and New-Zealand 15 January at 1500 UTC (CALIOP orbit N1, 2022; Sellitto et al., 2022, Figure S1 in Supporting Information S1). According to CALIOP, this layer shows linear particle depolarization ratio around 30%. At Reunion, only the 355 nm lidar offered a sufficient signal to assess the extinction, AOD and LR of N1 (Figures 2a–2c).

On Figures 2b and 2c the bulk of N1 appears around 34 km. The lidar-derived LR is surprisingly high (129 sr), and the associated uncertainty (74 sr) highlights the difficulty of obtaining a trustworthy characterization of this layer. Nonetheless, this value is indicative of a fine aerosol with probable absorption capabilities. While the ash and ice component of the initial plume stayed local and dissipated within few hours according to Sellitto et al. (2022), a mixture with remaining fine ash cannot be excluded for this high-altitude layer.

Two days later, N2 is located between 27 and 30 km (Figures 2d–2f). It is exceptionally thick, both geometrically (2–3 km) and optically, with a night-averaged AOD over 0.4 at 355 nm and a maximum AOD reaching 0.84 at 532 nm (Table 1). To our knowledge, this is unprecedentedly observed in the stratosphere. It doubles the value of 0.4 measured at Mauna Loa Observatory 90 days after the Pinatubo eruption (Antuña et al., 2002). Accordingly, the peak value of SR up to 404 at 532 nm (107 at 355 nm) should also be noted as what could be the greatest stratospheric perturbation by aerosol ever recorded at that altitude. N2 is stratified, presenting an increasing aerosol density with altitude. It is eventually caped at 30 km with a drastic decrease in extinction of four orders of magnitude within a few hundred meters.

The LR at 532 nm (69 ± 11, see Table 1) is characteristic of volcanic sulfates (Lopes et al., 2019 and references therein). At 355 nm, the LR is substantially lower (30 ± 2) and does not comply with the majority of the previous findings showing comparable LR for volcanic sulfates at these two wavelengths.

A cloud-free context permitted a night-long monitoring of N3, another dense layer between 24 and 28 km presenting values of AEC reaching 0.41 km^{-1} at 355 nm (Table 1). Even if they share remarkable values of AEC

and AOD and close LR estimates, N2 and N3 are distinct. The different timing of passage, and their contours argue in favor of two independent layers (Figure 1a). This separation is also corroborated by CALIOP (Legras et al., 2022), which sampled that double layer several times between 16 and 19 January. Also, unlike N1, all the following layers share near zero CALIOP-derived depolarization values indicating spherical aerosol shapes (Legras et al., 2022).

N3 seems to end with the beginning of N4 appearing lower in altitude (~22 km, Figure 1a). N4 is a stack of thin layers, followed the subsequent nights by N5 to N8 which tend to be lower in altitude and eventually decrease in terms of AOD. Table 1 covers in detail the properties of the plume.

As expected from Figure 1, the stratospheric AOD is extremely variable during the plume overpass. It ranges between almost four orders of magnitude with background values around 10^{-4} and maxima over 0.5 at both wavelengths. Interestingly, the maximum AOD is reached at 532 nm, rather than at 355 nm, as expected for most aerosol types. This implies a negative AE. It is very rare to find negative AE, only a few articles document such values and exclusively for large dust particles of pure dry volcanic ash (e.g., Fernández et al., 2019; Lopes et al., 2019; Rizzolo et al., 2017). Sicard et al. (2012) reported near zero AE associated with fresh sulfates aerosols after Eyjafjallajökull eruption above Spain, nevertheless the significantly negative AE recorded above Reunion are surprising. AERONET measurements (Holben et al., 1998) at the Maïdo station also show negative AE between 380 and 500 nm and even between 440 and 675 nm on 22 January as displayed in Figure S1 in Supporting Information S1.

The relatively high uncertainty on the computation AE with respect to AOD uncertainties for close wavelengths is also to be noted. A computation of these potential errors is proposed in Figure S2 in Supporting Information S1. The uncertainties for our estimates are reported in table 1 and correspond to AOD uncertainties below 35% for N2 and N3.

AE are plotted with their corresponding LR at 355 nm in Figure 3a. This graphic presentation highlights distinct aerosol clusters in the LR/AE plane. Taking into account the uncertainties in these values, only N6 stands out. We can still note a linear trend of the AE over time, which is also corroborated by collocated AERONET records at Maïdo (Figure S1 in Supporting Information S1). Known to be inversely proportional to the particle size (Schuster et al., 2006), the lidar-derived AE tends to indicate an aerosol size distribution driven by coarse mode (N2–N5), followed by a value (1.2, N6) more typical of average ash free volcanic particles (Sellitto et al., 2017). However, previous findings on the size distribution of the layers N4 and N5 (Kloss et al., 2022) show that the size distribution is driven by a fine mode populated by submicron particles. Furthermore, AERONET also attribute the majority of the columnar AOD to the fine mode (see Figure S2 of Sellitto et al., 2022).

To investigate these un-precedented results, we used a Mie code to test the reproducibility of such values.

Our hypotheses were as follows:

1. Spherical particles, as mentioned in earlier HTHH studies (Legras et al., 2022; Taha et al., 2022)
2. A monomodal lognormal size distribution often reported by in situ measurements on stratospheric balloons, and defined by its modal radius and dispersion (Chazette et al., 1995)
3. An aerosol mixture with the properties of sulfates particles that is, a real/imaginary part of the refractive index of $1.44/-5.10^{-3}$, respectively.

These hypotheses can be supported by the LR retrieved at 532 nm (~65 sr) which are coherent with the literature for volcanic aerosol driven by the presence of sulfates (Prata et al., 2017). However, the LR at 355 nm being almost two time smaller than what can be expected from the literature, this particle typing with LR is arguable.

The AE is given in Figure 3b against the modal radius and the dispersion of the lognormal size distribution. The modal radius and dispersion values matching with observations detailed in Table 1 (LR and AE) are contoured for the plumes N2–N6 where aerosol populations could exist under the previous hypotheses. One can note that above a modal radius of 0.3 µm, a monomodal sulfates mixture can have a negative AE. This latter result is presumably highlighting a shift between the extinction and scattering efficiencies at 355 and 532 nm for the N2 and N3 layers. On top of explaining the measured negative AE, this also helps to understand the low LR values at 355 nm. The extinction efficiency of a sulfate aerosol with a modal radius of 0.3–0.4 µm (~355 nm) is relatively lower at this wavelength compared to backscattering, decreasing the LR.

The plume sampled above Reunion being likely to comply with our hypotheses, we conclude that the mean radius of the particle tends to decrease by a factor of 2 from ~0.4 to ~0.2 µm while the monomodal size distribution gets more and more dispersed, the dispersion increasing from ~1.1 to ~1.8. Finally, given the dispersion values

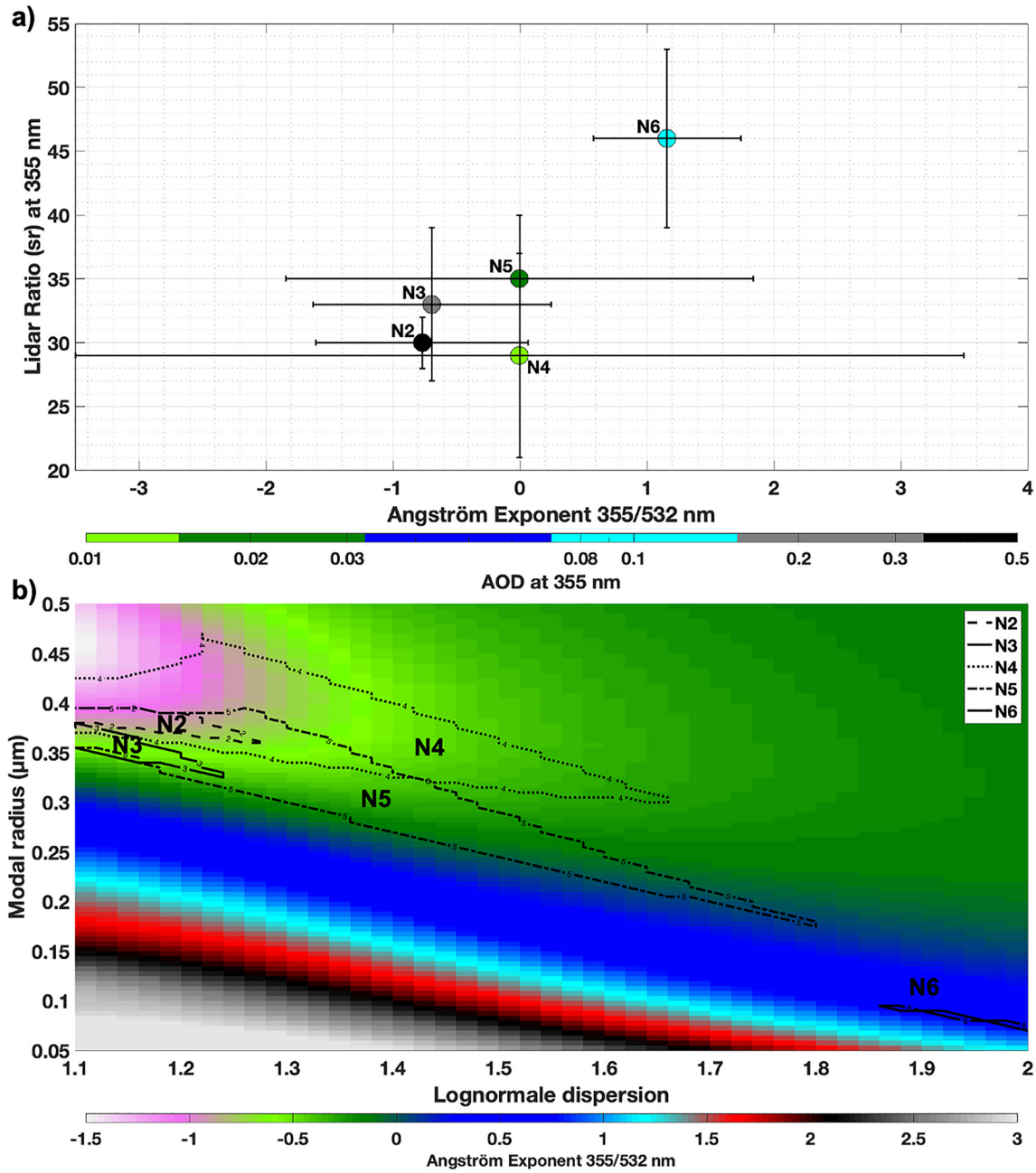

Figure 3. Scatterplot (a) of the Angström exponents (AEs) and lidar ratio at 355 nm for N2–N6. Lognormal dispersion and corresponding particle radius cross-section of AE (b), following Mie calculations for sulfates. The contours in (b) are constrained by the uncertainties and standard deviations values given in Table 1.

associated to N6, the tail of the plume probably does not comply with the monomodal hypothesis but could be a bimodal lognormal size distribution driven by fine mode (considering the AE values above 1).

5. Discussion and Summary

Lidar measurements performed over Reunion during the first passage of the stratospheric aerosol plume emanating from the HTHH volcano eruption show a plume structure marked by a very wide altitude range (18–36 km) over time.

The highest aerosol layer (N1) is observed as high as 36 km, a record-breaking altitude for ground-based lidar observations that is to be linked to the exceptional magnitude of this eruption. The altitude of the plume was

decreasing with time as it passed over Reunion due to strong wind gradients in the stratosphere, bending the initial eruptive column.

N1 presents aerosol optical properties which are specific to this eruption. In fact, the underwater caldera of the volcano and the power of the blast could have initially lifted water and gases suffering rapid thermodynamics changes that could result in a complex mixing of aerosol including non-spherical particles such as ashes and ice crystals (Khaykin et al., 2022; Sellitto et al., 2022). Hence, we cannot determine the nature of aerosol based solely on lidar measurements at 355 nm. However, the N2–N6 layers turned out to be well sampled by both lidars. The synergy between these measurements allows to infer their optical properties more extensively.

First, the AOD values recorded above Reunion are, as far as we know, the highest ever recorded in the stratosphere (0.83 at 532 nm, peak SR of 403). Following the LR values, especially at 532 nm (∼65 sr), as well as the known typical optical properties of volcanic aerosol, we expected to have observed a majority of sulfate particles. The unprecedented low AE (down to ∼−0.8) values can be explained by Mie theory computations with monomode lognormal size distributions of sulfate particles, with radii exceeding 0.3 μm in most of the cases (N2–N4). Our calculations show that these radii tend to decrease while the dispersion on the lognormal tend to increase. This also explain the relatively low LR at 355 nm and its tendency to increase inversely with modal radii of aerosols.

These unusual characteristics for volcanic aerosols likely result from the fast conversion of SO_2 to H_2SO_4 (Carn et al., 2022; Zhu et al., 2022) in presence of a high water vapor availability (Vömel et al., 2022). This fast chemistry in the fresh plume with the higher layer being the wetter ended with the AE increasing tendency over time and altitude. Note that the relatively high uncertainty on the AE associated with such a close pair of wavelengths (355/532 nm, see Text S2 in Supporting Information S1) is compensated for layers N2 and N3 by low AOD uncertainties. As a result, it interestingly demonstrates that these layers have a greater efficiency to extinct the visible light than the UV light.

To conclude, this study presents original observations of an exceptional volcanic event resulting in an unprecedented aerosol burden at those altitudes. Considering the lidar-derived optical aerosol properties, we can assess some microphysical properties of the volcanic aerosol layers and explain their unusual optical behavior. This data set is also continuing to grow as observations are routinely made, it will constitute an opportunity to follow up on the long-term evolution of this stratospheric plume and bring constraint on aerosol modeling following such a rare event.

Data Availability Statement

The data used in this study are publicly accessible via this webpage: https://geosur.osureunion.fr/geonetwork/srv/eng/catalog.search#/metadata/f2c35798-47b7-433c-8927-46cf7babca83. The L2 ready-to-use data set in netCDF format is available through this link: https://doi.org/10.5281/zenodo.7790283.

Acknowledgments
The authors gratefully acknowledge the Region Reunion, the CNRS, Météo France and the Université de la Réunion for support and contribution within the research infrastructure OPAR (Observatoire de Physique de l'Atmosphère à la Réunion). We also sincerely want to thank all the individuals for their contribution during the campaign to help with the measurements: J.-P. Cammas, E. Golubic, Y. Hello, P. Hernandez, T. Portafaix, M. Ranaivombola. We also acknowledge the French Centre for Spatial Studies (CNES) for providing a research grant to the first author.

References

Amores, A., Monserrat, S., Marcos, M., Argüeso, D., Villalonga, J., Jordà, G., & Gomis, D. (2022). Numerical simulation of atmospheric lamb waves generated by the 2022 Hunga-Tonga volcanic eruption. *Geophysical Research Letters*, *49*(6), e2022GL098240. https://doi.org/10.1029/2022GL098240

Angell, J. K. (1993). Comparison of stratospheric warming following Agung, El Chichon and Pinatubo volcanic eruptions. *Geophysical Research Letters*, *20*(8), 715–718. https://doi.org/10.1029/93GL00366

Antuña, J. C., Robock, A., Stenchikov, G. L., Thomason, L. W., & Barnes, J. E. (2002). Lidar validation of SAGE II aerosol measurements after the 1991 Mount Pinatubo eruption. *Journal of Geophysical Research*, *107*(D14), ACL3-1–ACL3-11. https://doi.org/10.1029/2001JD001441

Baray, J.-L., Courcoux, Y., Keckhut, P., Portafaix, T., Tulet, P., Cammas, J.-P., et al. (2013). Maïdo observatory: A new high-altitude station facility at Reunion Island (21°S, 55°E) for long-term atmospheric remote sensing and in situ measurements. *Atmospheric Measurement Techniques*, *6*(10), 2865–2877. https://doi.org/10.5194/amt-6-2865-2013

Boville, B. A., Holton, J. R., & Mote, P. W. (1991). Simulation of the Pinatubo aerosol cloud in general circulation model. *Geophysical Research Letters*, *18*(12), 2281–2284. https://doi.org/10.1029/91GL02778

Caliop orbit N1, N. (2022). CALIOP orbit N1. Retrieved from https://www-calipso.larc.nasa.gov/products/lidar/browse_images/show_detail.php?s=expedited&v=V3-30&browse_date=2022-01-15&orbit_time=15-00-00&page=1&granule_name=CAL_LID_L1_Exp-Prov-V3-41.2022-01-15T15-00-00Z.hdf

Carn, S. A., Krotkov, N. A., Fisher, B. L., & Li, C. (2022). Out of the blue: Volcanic SO_2 emissions during the 2021–2022 eruptions of Hunga Tonga—Hunga Ha'apai (Tonga). *Frontiers of Earth Science*, *10*, 976962. https://doi.org/10.3389/feart.2022.976962

Carr, J. L., Horváth, Á., Wu, D. L., & Friberg, M. D. (2022). Stereo plume height and motion retrievals for the record-setting Hunga Tonga-Hunga Ha'apai eruption of 15 January 2022. *Geophysical Research Letters*, *49*(9), e2022GL098131. https://doi.org/10.1029/2022GL098131

Carvajal, M., Sepúlveda, I., Gubler, A., & Garreaud, R. (2022). Worldwide signature of the 2022 Tonga volcanic Tsunami. *Geophysical Research Letters*, *49*(6), e2022GL098153. https://doi.org/10.1029/2022GL098153

Chazette, P., Bocquet, M., Royer, P., Winiarek, V., Raut, J.-C., Labazuy, P., et al. (2012). Eyjafjallajökull ash concentrations derived from both lidar and modeling. *Journal of Geophysical Research*, *117*(D20), D00U14. https://doi.org/10.1029/2011JD015755

Chazette, P., David, C., Lefrère, J., Godin, S., Pelon, J., & Mégie, G. (1995). Comparative lidar study of the optical, geometrical, and dynamical properties of stratospheric post-volcanic aerosols, following the eruptions of El Chichon and Mount Pinatubo. *Journal of Geophysical Research*, *100*(D11), 23195–23207. https://doi.org/10.1029/95JD02268

Chazette, P., Totems, J., Ancellet, G., Pelon, J., & Sicard, M. (2016). Temporal consistency of lidar observations during aerosol transport events in the framework of the ChArMEx/ADRIMED campaign at Minorca in June 2013. *Atmospheric Chemistry and Physics*, *16*(5), 2863–2875. https://doi.org/10.5194/acp-16-2863-2016

DeFoor, T. E., Robinson, E., & Ryan, S. (1992). Early lidar observations of the June 1991 Pinatubo eruption plume at Mauna Loa observatory, Hawaii. *Geophysical Research Letters*, *19*(2), 187–190. https://doi.org/10.1029/91GL02791

Delmas, R. J., Kirchner, S., Palais, J. M., & Petit, J.-R. (1992). 1000 years of explosive volcanism recorded at the South Pole. *Tellus B: Chemical and Physical Meteorology*, *44*(4), 335–350. https://doi.org/10.3402/tellusb.v44i4.15461

Dhomse, S. S., Mann, G. W., Antuña Marrero, J. C., Shallcross, S. E., Chipperfield, M. P., Carslaw, K. S., et al. (2020). Evaluating the simulated radiative forcings, aerosol properties, and stratospheric warmings from the 1963 Mt Agung, 1982 El Chichón, and 1991 Mt Pinatubo volcanic aerosol clouds. *Atmospheric Chemistry and Physics*, *20*(21), 13627–13654. https://doi.org/10.5194/acp-20-13627-2020

Dionisi, D., Keckhut, P., Courcoux, Y., Hauchecorne, A., Porteneuve, J., Baray, J. L., et al. (2015). Water vapor observations up to the lower stratosphere through the Raman lidar during the Maïdo Lidar Calibration Campaign. *Atmospheric Measurement Techniques*, *8*(3), 1425–1445. https://doi.org/10.5194/amt-8-1425-2015

Duflot, V., Baray, J.-L., Payen, G., Marquestaut, N., Posny, F., Metzger, J.-M., et al. (2017). Tropospheric ozone profiles by DIAL at Maïdo observatory (Reunion Island): System description, instrumental performance and result comparison with ozone external data set. *Atmospheric Measurement Techniques*, *10*(9), 3359–3373. https://doi.org/10.5194/amt-10-3359-2017

Duflot, V., Royer, P., Chazette, P., Baray, J.-L., Courcoux, Y., & Delmas, R. (2011). Marine and biomass burning aerosols in the southern Indian Ocean: Retrieval of aerosol optical properties from shipborne lidar and Sun photometer measurements. *Journal of Geophysical Research*, *116*(D18), D18208. https://doi.org/10.1029/2011JD015839

Fernández, A. J., Sicard, M., Costa, M. J., Guerrero-Rascado, J. L., Gómez-Amo, J. L., Molero, F., et al. (2019). Extreme, wintertime Saharan dust intrusion in the Iberian Peninsula: Lidar monitoring and evaluation of dust forecast models during the February 2017 event. *Atmospheric Research*, *228*, 223–241. https://doi.org/10.1016/j.atmosres.2019.06.007

Gobbi, G. P., Congeduti, F., & Adriani, A. (1992). Early stratospheric effects of the Pinatubo eruption. *Geophysical Research Letters*, *19*(10), 997–1000. https://doi.org/10.1029/92GL01038

Graft, H.-F., Kirchner, I., Robock, A., & Schult, I. (1993). Pinatubo eruption winter climate effects: Model versus observations. *Climate Dynamics*, *9*(2), 81–93. https://doi.org/10.1007/BF00210011

Guo, S., Bluth, G. J. S., Rose, W. I., Watson, I. M., & Prata, A. J. (2004). Re-evaluation of SO_2 release of the 15 June 1991 Pinatubo eruption using ultraviolet and infrared satellite sensors. *Geochemistry, Geophysics, Geosystems*, *5*(4), Q04001. https://doi.org/10.1029/2003GC000654

Hersbach, H., Bell, B., Berrisford, P., Hirahara, S., Horányi, A., Muñoz-Sabater, J., et al. (2020). The ERA5 global reanalysis. *Quarterly Journal of the Royal Meteorological Society*, *146*(730), 1999–2049. https://doi.org/10.1002/qj.3803

Holben, B. N., Eck, T. F., Slutsker, I., Tanré, D., Buis, J. P., Setzer, A., et al. (1998). AERONET—A federated instrument network and data archive for aerosol characterization. *Remote Sensing of Environment*, *66*(1), 1–16. https://doi.org/10.1016/S0034-4257(98)00031-5

Khaykin, S., Legras, B., Bucci, S., Sellitto, P., Isaksen, L., Tencé, F., et al. (2020). The 2019/20 Australian wildfires generated a persistent smoke-charged vortex rising up to 35 km altitude. *Communications Earth & Environment*, *1*(1), 1–12. https://doi.org/10.1038/s43247-020-00022-5

Khaykin, S., Podglajen, A., Ploeger, F., Grooß, J.-U., Tence, F., Bekki, S., et al. (2022). Global perturbation of stratospheric water and aerosol burden by Hunga eruption. *Communications Earth & Environment*, *3*(1), 1–15. https://doi.org/10.1038/s43247-022-00652-x

Klett, J. D. (1985). Lidar inversion with variable backscatter/extinction ratios. *Applied Optics*, *24*(11), 1638–1643. https://doi.org/10.1364/AO.24.001638

Kloss, C., Sellitto, P., Renard, J., Baron, A., Bègue, N., Legras, B., et al. (2022). Aerosol characterization of the stratospheric plume from the volcanic eruption at Hunga Tonga 15 January 2022. *Geophysical Research Letters*, *49*(16), e2022GL099394. https://doi.org/10.1029/2022GL099394

Krishnamohan, K. P. S. P., Bala, G., Cao, L., Duan, L., & Caldeira, K. (2019). Climate system response to stratospheric sulfate aerosols: Sensitivity to altitude of aerosol layer. *Earth System Dynamics*, *10*(4), 885–900. https://doi.org/10.5194/esd-10-885-2019

Legras, B., Duchamp, C., Sellitto, P., Podglajen, A., Carboni, E., Siddans, R., et al. (2022). The evolution and dynamics of the Hunga Tonga–Hunga Ha'apai sulfate aerosol plume in the stratosphere. *Atmospheric Chemistry and Physics*, *22*(22), 14957–14970. https://doi.org/10.5194/acp-22-14957-2022

Lopes, F. J. S., Silva, J. J., Antuña Marrero, J. C., Taha, G., & Landulfo, E. (2019). Synergetic aerosol layer observation after the 2015 Calbuco volcanic eruption event. *Remote Sensing*, *11*(2), 195. https://doi.org/10.3390/rs11020195

Mallet, M., Chazette, P., Dulac, F., Formenti, P., Di Biagio, C., Denjean, C., & Chiapello, I. (2022). Aerosol optical properties. In F. Dulac, S. Sauvage, & E. Hamonou (Eds.), *Atmospheric chemistry in the Mediterranean region: Volume 2—From air pollutant sources to impacts* (pp. 253–284). Springer International Publishing. https://doi.org/10.1007/978-3-030-82385-6_14

McCormick, M. P., Thomason, L. W., & Trepte, C. R. (1995). Atmospheric effects of the Mt Pinatubo eruption. *Nature*, *373*(6513), 399–404. https://doi.org/10.1038/373399a0

McCormick, M. P., & Veiga, R. E. (1992). SAGE II measurements of early Pinatubo aerosols. *Geophysical Research Letters*, *19*(2), 155–158. https://doi.org/10.1029/91GL02790

Minnis, P., Harrison, E. F., Stowe, L. L., Gibson, G. G., Denn, F. M., Doelling, D. R., & Smith, W. L. (1993). Radiative climate forcing by the Mount Pinatubo eruption. *Science*, *259*(5100), 1411–1415. https://doi.org/10.1126/science.259.5100.1411

Müller, D., Ansmann, A., Mattis, I., Tesche, M., Wandinger, U., Althausen, D., & Pisani, G. (2007). Aerosol-type-dependent lidar ratios observed with Raman lidar. *Journal of Geophysical Research*, *112*(D16), D16202. https://doi.org/10.1029/2006JD008292

Platt, C. M. R. (1973). Lidar and Radiometric observations of Cirrus clouds. *Journal of the Atmospheric Sciences*, *30*(6), 1191–1204. https://doi.org/10.1175/1520-0469(1973)030<1191:LAROOC>2.0.CO;2

Podglajen, A., Le Pichon, A., Garcia, R. F., Gérier, S., Millet, C., Bedka, K., et al. (2022). Stratospheric balloon observations of Infrasound waves from the 15 January 2022 Hunga eruption, Tonga. *Geophysical Research Letters*, *49*(19), e2022GL100833. https://doi.org/10.1029/2022GL100833

Poli, P., & Shapiro, N. M. (2022). Rapid characterization of large volcanic eruptions: Measuring the impulse of the Hunga Tonga Ha'apai explosion from teleseismic waves. *Geophysical Research Letters*, *49*(8), e2022GL098123. https://doi.org/10.1029/2022GL098123

Prata, A. T., Young, S. A., Siems, S. T., & Manton, M. J. (2017). Lidar ratios of stratospheric volcanic ash and sulfate aerosols retrieved from CALIOP measurements. *Atmospheric Chemistry and Physics*, *17*(13), 8599–8618. https://doi.org/10.5194/acp-17-8599-2017

Proud, S. R., Prata, A. T., & Schmauß, S. (2022). The January 2022 eruption of Hunga Tonga-Hunga Ha'apai volcano reached the mesosphere. *Science*, *378*(6619), 554–557. https://doi.org/10.1126/science.abo4076

Rizzolo, J. A., Barbosa, C. G. G., Borillo, G. C., Godoi, A. F. L., Souza, R. A. F., Andreoli, R. V., et al. (2017). Soluble iron nutrients in Saharan dust over the central Amazon rainforest. *Atmospheric Chemistry and Physics*, *17*(4), 2673–2687. https://doi.org/10.5194/acp-17-2673-2017

Robock, A. (2015). Chapter 53—Climatic impacts of volcanic eruptions. In H. Sigurdsson (Ed.), *The encyclopedia of volcanoes* (2nd ed., pp. 935–942). Academic Press. https://doi.org/10.1016/B978-0-12-385938-9.00053-5

Robock, A., & Mao, J. (1995). The volcanic signal in surface temperature observations. *Journal of Climate*, *8*(5), 1086–1103. https://doi.org/10.1175/1520-0442(1995)008<1086:TVSIST>2.0.CO;2

Schuster, G. L., Dubovik, O., & Holben, B. N. (2006). Angstrom exponent and bimodal aerosol size distributions. *Journal of Geophysical Research*, *111*(D7), D07207. https://doi.org/10.1029/2005JD006328

Sellitto, P., Podglajen, A., Belhadji, R., Boichu, M., Carboni, E., Cuesta, J., et al. (2022). The unexpected radiative impact of the Hunga Tonga eruption of 15th January 2022. *Communications Earth & Environment*, *3*(1), 1–10. https://doi.org/10.1038/s43247-022-00618-z

Sellitto, P., Salerno, G., La Spina, A., Caltabiano, T., Terray, L., Gauthier, P.-J., & Briole, P. (2017). A novel methodology to determine volcanic aerosols optical properties in the UV and NIR and Ångström parameters using Sun photometry. *Journal of Geophysical Research: Atmospheres*, *122*(18), 9803–9815. https://doi.org/10.1002/2017JD026723

Sicard, M., Guerrero-Rascado, J. L., Navas-Guzmán, F., Preißler, J., Molero, F., Tomás, S., et al. (2012). Monitoring of the Eyjafjallajökull volcanic aerosol plume over the Iberian Peninsula by means of four EARLINET lidar stations. *Atmospheric Chemistry and Physics*, *12*(6), 3115–3130. https://doi.org/10.5194/acp-12-3115-2012

Taha, G., Loughman, R., Colarco, P. R., Zhu, T., Thomason, L. W., & Jaross, G. (2022). Tracking the 2022 Hunga Tonga-Hunga Ha'apai aerosol cloud in the upper and middle stratosphere using space-based observations. *Geophysical Research Letters*, *49*(19), e2022GL100091. https://doi.org/10.1029/2022GL100091

Tejedor, E., Steiger, N., Smerdon, J. E., Serrano-Notivoli, R., & Vuille, M. (2021). Global temperature responses to large tropical volcanic eruptions in Paleo data assimilation products and climate model simulations over the last millennium. *Paleoceanography and Paleoclimatology*, *36*(4), e2020PA004128. https://doi.org/10.1029/2020PA004128

Vérèmes, H., Payen, G., Keckhut, P., Duflot, V., Baray, J.-L., Cammas, J.-P., et al. (2019). Validation of the water vapor profiles of the Raman lidar at the Maïdo observatory (Reunion Island) Calibrated with global Navigation satellite system integrated water vapor. *Atmosphere*, *10*(11), 713. https://doi.org/10.3390/atmos10110713

Vergoz, J., Hupe, P., Listowski, C., Le Pichon, A., Garcés, M. A., Marchetti, E., et al. (2022). IMS observations of infrasound and acoustic-gravity waves produced by the January 2022 volcanic eruption of Hunga, Tonga: A global analysis. *Earth and Planetary Science Letters*, *591*, 117639. https://doi.org/10.1016/j.epsl.2022.117639

Vernier, J.-P., Thomason, L. W., Pommereau, J.-P., Bourassa, A., Pelon, J., Garnier, A., et al. (2011). Major influence of tropical volcanic eruptions on the stratospheric aerosol layer during the last decade. *Geophysical Research Letters*, *38*(12), L12807. https://doi.org/10.1029/2011GL047563

Vömel, H., Evan, S., & Tully, M. (2022). Water vapor injection into the stratosphere by Hunga Tonga-Hunga Ha'apai. *Science*, *377*(6613), 1444–1447. https://doi.org/10.1126/science.abq2299

Winker, D. M., Pelon, J. R., & McCormick, M. P. (2003). The CALIPSO mission: Spaceborne lidar for observation of aerosols and clouds. In U. N. Singh, T. Itabe, & Z. Liu (Eds.) *Presented at the third international Asia-pacific environmental remote sensing remote sensing of the atmosphere, Ocean, Environment, and Space* (p. 1). https://doi.org/10.1117/12.466539

Yu, P., Toon, O. B., Bardeen, C. G., Zhu, Y., Rosenlof, K. H., Portmann, R. W., et al. (2019). Black carbon lofts wildfire smoke high into the stratosphere to form a persistent plume. *Science*, *365*(6453), 587–590. https://doi.org/10.1126/science.aax1748

Yuen, D. A., Scruggs, M. A., Spera, F. J., Zheng, Y., Hu, H., McNutt, S. R., et al. (2022). Under the surface: Pressure-induced planetary-scale waves, volcanic lightning, and gaseous clouds caused by the submarine eruption of Hunga Tonga-Hunga Ha'apai volcano. *Earthquake Research Advances*, *2*(3), 100134. https://doi.org/10.1016/j.eqrea.2022.100134

Zhu, Y., Bardeen, C. G., Tilmes, S., Mills, M. J., Wang, X., Harvey, V. L., et al. (2022). Perturbations in stratospheric aerosol evolution due to the water-rich plume of the 2022 Hunga-Tonga eruption. *Communications Earth & Environment*, *3*(1), 1–7. https://doi.org/10.1038/s43247-022-00580-w